HEAVY QUARK PRODUCTION IN THE ACOT SCHEME BEYOND NLO*

T. Stavreva[a], F.I. Olness[b], I. Schienbein[a], T. Ježo[a], A. Kusina[b]
K. Kovařík[c], J.Y. Yu[a,b]

[a]Laboratoire de Physique Subatomique et de Cosmologie
Université Joseph Fourier/CNRS-IN2P3/INPG
53 Avenue des Martyrs, 38026 Grenoble, France
[b]Southern Methodist University, Dallas, TX 75275, USA
[c]Institute for Theoretical Physics, Karlsruhe Institute of Technology
76128 Karlsruhe, Germany

(Received May 14, 2012)

We compute the structure functions F_2 and F_L in the ACOT scheme for heavy quark production. We use the complete ACOT results to NLO, and make use of the $\overline{\rm MS}$ massless results at NNLO and N^{3}LO to estimate the higher order mass-dependent corrections. We show numerically that the dominant heavy quark mass effects can be taken into account using massless Wilson coefficients together with an appropriate rescaling prescription. Combining the exact NLO ACOT scheme with these expressions should provide a good approximation to the full calculation in the ACOT scheme at NNLO and N^{3}LO.

DOI:10.5506/APhysPolB.43.1607
PACS numbers: 12.38.–t, 12.38.Bx, 12.39.St, 13.60.–r

1. Introduction

The production of heavy quarks in high energy processes has become an increasingly important subject of study both theoretically and experimentally. The theory of heavy quark production in perturbative Quantum Chromodynamics (pQCD) is more challenging than that of light parton (jet) production because of the new physics issues brought about by the additional heavy quark mass scale. The correct theory must properly take into account the changing role of the heavy quark over the full kinematic range of the relevant process from the threshold region (where the quark behaves like

* Presented by A. Kusina at the Cracow Epiphany Conference on Present and Future of B Physics, Cracow, Poland, January 9–11, 2012.

a typical "heavy particle") to the asymptotic region (where the same quark behaves effectively like a parton, similar to the well known light quarks $\{u, d, s\}$).

With the ever-increasing precision of experimental data and the progression of theoretical calculations and parton distribution function (PDF) evolution to next-to-next-to-leading order (NNLO) of QCD, there is a clear need to formulate and also implement the heavy quark schemes at this order and beyond. The most important case is arguably the heavy quark treatment in inclusive deep-inelastic scattering (DIS) since the very precise HERA data for DIS structure functions and cross sections form the backbone of any modern global analysis of PDFs. Here, the heavy quarks contribute up to 30% or 40% to the structure functions at small momentum fractions x. Extending the heavy quark schemes to higher orders is, therefore, necessary for extracting precise PDFs, and this is a prerequisite for precise predictions of observables at the LHC. However, we would like to also stress the theoretical importance of having a general pQCD framework that includes heavy quarks and is valid to all orders in perturbation theory over a wide range of hard energy scales.

An example, where higher order corrections are particularly important is the structure function $F_{\rm L}$ in DIS. The leading order ($\mathcal{O}(\alpha_{\rm S}^0)$) contribution to this structure function vanishes for massless quarks due to helicity conservation (Callan–Gross relation). This has several consequences: (1) $F_{\rm L}$ is useful for constraining the gluon PDF via the dominant subprocess $\gamma^* g \to q\bar{q}$. (2) The heavy quark mass effects of order $\mathcal{O}(\frac{m^2}{Q^2})$ are relatively more pronounced[1]. (3) Since the first non-vanishing contribution to $F_{\rm L}$ is next-to-leading order (up to mass effects), the NNLO and N^{3}LO corrections are more important than for F_2. In Fig. 1, we show a comparison of different theoretical calculations of $F_{\rm L}$ with preliminary HERA data [2]. As can be seen, in particular at small Q^2 (*i.e.* small x), there are considerable differences between the predictions.

The purpose of this paper is to calculate the leading twist neutral current DIS structure functions F_2 and $F_{\rm L}$ in the ACOT factorization scheme up to order $\mathcal{O}(\alpha_{\rm S}^3)$ (N^{3}LO) and to estimate the error due to approximating the heavy quark mass terms $\mathcal{O}(\alpha_{\rm S}^2 \times \frac{m^2}{Q^2})$ and $\mathcal{O}(\alpha_{\rm S}^3 \times \frac{m^2}{Q^2})$ in the higher order corrections. The results of this study form the basis for using the ACOT scheme in NNLO global analyses and for future comparisons with precision data for DIS structure functions.

[1] Similar considerations also hold for target mass corrections (TMC) and higher twist terms. We focus here mainly on the kinematic region $x < 0.1$, where TMC are small [1]. An inclusion of higher twist terms is beyond the scope of this study.

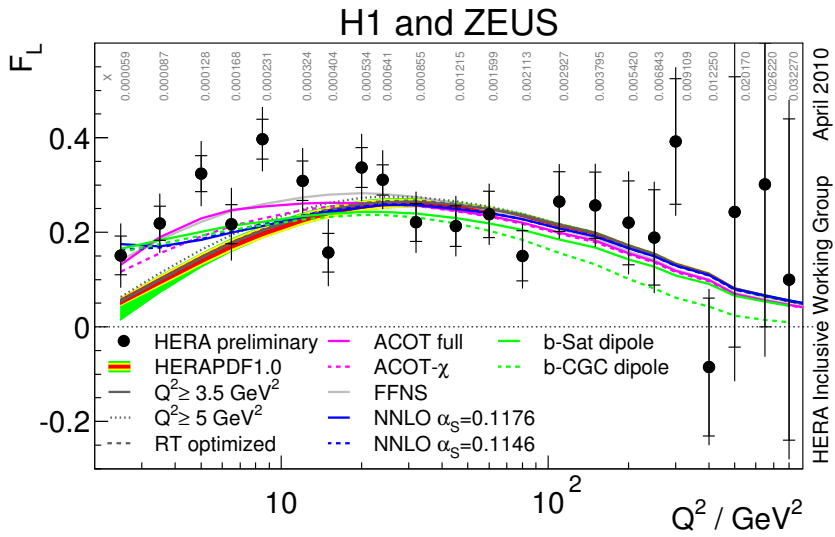

Fig. 1. F_L *vs.* Q from combined HERA-I inclusive deep inelastic cross sections measured by the H1 and ZEUS collaborations. Figure taken from Ref. [2].

This paper is organized as follows. In Sec. 2, we review theoretical approaches to include heavy flavors in QCD calculations. Particular emphasis is put on the ACOT scheme which is a minimal extension of the $\overline{\text{MS}}$ scheme. In Sec. 3, we present the prescription for constructing the approximate DIS structure functions in the ACOT scheme up to $\mathcal{O}(\alpha_S^3)$ order. The corresponding numerical results are presented in Sec. 4. Finally, in Sec. 5 we summarize the main results. This work is based on Ref. [3], and further details can be found therein.

2. Review of theoretical methods

We review theoretical methods which have been advanced to improve existing QCD calculations of heavy quark production, and the impact on recent experimental results.

2.1. ACOT Scheme

The ACOT renormalization scheme [4, 5] provides a mechanism to incorporate the heavy quark mass into the theoretical calculation of heavy quark production both kinematically and dynamically. In 1998, Collins [6] extended the factorization theorem to address the case of heavy quarks; this work provided the theoretical foundation that allows us to reliably compute heavy quark processes throughout the full kinematic realm.

If we consider the DIS production of heavy quarks at $\mathcal{O}(\alpha_S^1)$ this involves the LO $QV \to Q$ process and the NLO $gV \to Q\bar{Q}$ process[2]. The key ingredient provided by the ACOT scheme is the subtraction term (SUB) which removes the "double counting" arising from the regions of phase space, where the LO and NLO contributions overlap. Specifically, at NLO order, we can express the total result as a sum of

$$\sigma_{\rm TOT} = \sigma_{\rm LO} + \{\sigma_{\rm NLO} - \sigma_{\rm SUB}\} \,, \tag{1}$$

where the subtraction term for the gluon-initiated processes is

$$\sigma_{\rm SUB} = f_g \otimes \tilde{P}_{g\to Q} \otimes \sigma_{QV\to Q} \,. \tag{2}$$

$\sigma_{\rm SUB}$ represents a gluon emitted from a proton (f_g) which undergoes a collinear splitting to a heavy quark ($\tilde{P}_{g\to Q}$) convoluted with the LO quark–boson scattering $\sigma_{QV\to Q}$. Here, $\tilde{P}_{g\to Q}(x,\mu) = \frac{\alpha_S}{2\pi} \ln(\mu^2/m^2)\, P_{g\to Q}(x)$, where $P_{g\to Q}(x)$ is the usual $\overline{\rm MS}$ splitting kernel, m is the quark mass and μ is the renormalization scale which we typically choose to be $\mu = Q$.

An important feature of the ACOT scheme is that it reduces to the appropriate limit both as $m \to 0$ and $m \to \infty$ as we illustrate below. Specifically, in the limit where the quark Q is relatively heavy compared to the characteristic energy scale ($\mu \lesssim m$), we find $\sigma_{\rm LO} \sim \sigma_{\rm SUB}$ such that $\sigma_{\rm TOT} \sim \sigma_{\rm NLO}$. In this limit, the ACOT result naturally reduces to the Fixed-Flavor-Number-Scheme (FFNS) result. In the FFNS, the heavy quark is treated as being extrinsic to the hadron, and there is no corresponding heavy quark PDF ($f_Q \sim 0$); thus $\sigma_{\rm LO} \sim 0$. We also have $\sigma_{\rm SUB} \sim 0$ because this is proportional to $\ln(\mu^2/m^2)$. Thus, when the quark Q is heavy relative to the characteristic energy scale μ, the ACOT result reduces to $\sigma_{\rm TOT} \sim \sigma_{\rm NLO}$.

Conversely, in the limit where the quark Q is relatively light compared to the characteristic energy scale ($\mu \gtrsim m$), we find that $\sigma_{\rm LO}$ yields the dominant part of the result, and the "formal" NLO $\mathcal{O}(\alpha_S)$ contribution $\{\sigma_{\rm NLO} - \sigma_{\rm SUB}\}$ is an $\mathcal{O}(\alpha_S)$ correction. In this limit, the ACOT result will reduce to the $\overline{\rm MS}$ Zero-Mass Variable-Flavor-Number-Scheme (ZM-VFNS) limit exactly without any finite renormalizations. The quark mass m no longer plays any dynamical role and purely serves as a regulator. The $\sigma_{\rm NLO}$ term diverges due to the internal exchange of the quark Q, and this singularity is canceled by $\sigma_{\rm SUB}$.

We illustrate the versatile role of the quark mass in Fig. 2 (a), where we display F_2^c as a function of Q calculated in the ZM-VFNS, FFNS, ACOT, and S-ACOT schemes. We see that the ACOT scheme coincides with the

[2] At NLO, there are corresponding quark-initiated terms; for simplicity we do not display them here, but they are fully contained in our calculations [7].

FFNS for small Q, and the ZM-VFNS for large Q. In Fig. 2 (b), we plot F_2^c as a function of the quark mass m for a fixed $Q = 10\,\text{GeV}$ for the $\overline{\text{MS}}$ ZM-VFNS and ACOT schemes. We observe that when m is within a decade or two of μ, the quark mass plays a dynamic role; however, for $m \ll \mu$, the quark mass purely serves as a regulator and the specific value is not important. Operationally, it means we can obtain the $\overline{\text{MS}}$ ZM-VFNS result either by *(i)* computing the terms using dimensional regularization and setting the regulator to zero, or *(ii)* by computing the terms using the quark mass as the regulator and then setting this to zero.

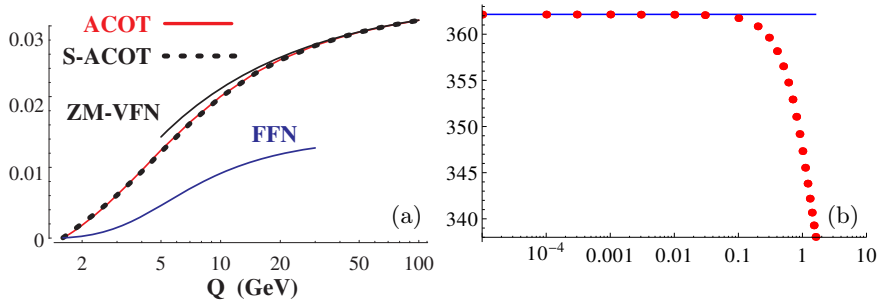

Fig. 2. (a) F_2^c for $x = 0.1$ for NLO DIS heavy quark production as a function of Q. We display calculations using the ACOT, S-ACOT, Fixed-Flavor Number Scheme (FFNS), and Zero-Mass Variable Flavor Number Scheme (ZM-VFNS). The ACOT and S-ACOT results are virtually identical. (b) Comparison of $F_2^c(x, Q)$ (scaled by 10^4) *vs.* the quark mass m in GeV for fixed $x = 0.1$ and $Q = 10\,\text{GeV}$. The full (red) dots are the full ACOT result, and the solid (blue) line is the massless $\overline{\text{MS}}$ result.

The ACOT scheme is minimal in the sense that the construction of the massive short distance cross sections does not need any observable-dependent extra contributions or any regulators to smooth the transition between the high and low scale regions. The ACOT prescription is: (a) calculate the massive partonic cross sections, and (b) perform the factorization using the quark mass as regulator.

It is in this sense that we claim the ACOT scheme is the minimal massive extension of the $\overline{\text{MS}}$ ZM-VFNS. In the limit $m/\mu \to 0$ it reduces exactly to the $\overline{\text{MS}}$ ZM-VFNS, in the limit $m/\mu \gtrsim 1$ the heavy quark decouples from the PDFs and we obtain exactly the FFNS for $m/\mu \gg 1$ and no finite renormalizations are needed.

2.2. S-ACOT

In a corresponding application, it was observed that the heavy quark mass could be set to zero in certain pieces of the hard scattering terms without any loss of accuracy. This modification of the ACOT scheme goes by the name Simplified-ACOT (S-ACOT) and can be summarized as follows [8].

S-ACOT: For hard-scattering processes with incoming heavy quarks or with internal on-shell cuts on a heavy quark line, the heavy quark mass can be set to zero ($m = 0$) for these pieces.

If we consider the case of NLO DIS heavy quark production, this means we can set $m = 0$ for the LO terms $\sigma_{QV\to Q}$ (incoming heavy quark), and for the SUB terms (on-shell cut on an internal heavy quark line). Hence, the only contribution which requires calculation with m retained is the NLO $gV \to Q\bar{Q}$ process. Figure 2 (a) displays a comparison of a calculation using the ACOT scheme with all masses retained *vs.* the S-ACOT scheme; as expected, these two results match throughout the full kinematic region.

It is important to note that the S-ACOT scheme is not an approximation; this is an exact renormalization scheme, extensible to all orders.

2.3. ACOT and χ-rescaling

As we have illustrated in Sec. 2.1, in the limit $Q^2 \gg m^2$ the mass simply plays the role of a regulator. In contrast, for $Q^2 \sim m^2$ the value of the mass is of consequence for the physics. The mass can enter dynamically in the hard-scattering matrix element, and can enter kinematically in the phase space of the process.

We will demonstrate that for the processes of interest the primary role of the mass is kinematic and not dynamic. It was this idea which was behind the original slow-rescaling prescription of [9] which considered DIS charm production (*e.g.*, $\gamma c \to c$) introducing the shift $x \to \chi = x[1 + (m_c/Q)^2]$. This prescription accounted for the charm quark mass by effectively reducing the phase space for the final state by an amount proportional to $(m_c/Q)^2$.

This idea was extended in the χ-scheme by realizing that (in most cases) in addition to the observed final-state charm quark, there is also an anti-charm quark in the beam fragments since all the charm quarks are ultimately produced by gluon splitting ($g \to c\bar{c}$) into a charm pair. For this case, the scaling variable becomes $\chi = x[1+(2m_c/Q)^2]$. This rescaling is implemented in the ACOT$_\chi$ scheme, for example [10,11,12][3]. The factor $(1+(2m_c)^2/Q^2)$ represents a kinematic suppression factor which will suppress the charm process relative to the lighter quarks. Additionally, the χ-scaling ensures the threshold kinematics ($W^2 > 4m^2 + M^2$) is satisfied; while it is important to satisfy this condition for large x, this may prove too restrictive at small x, where the HERA data are especially precise.

[3] Use of more general rescaling prescriptions have been discussed in Ref. [13].

To encompass all the above results, we can define a general scaling variable $\chi(n)$ as

$$\chi(n) = x\left[1 + \left(\frac{n\, m_c}{Q}\right)^2\right], \tag{3}$$

where $n = \{0, 1, 2\}$. Here, $n = 0$ corresponds to the massless result without rescaling, $n = 1$ corresponds to the original Barnett slow-rescaling, and $n = 2$ corresponds to the χ-rescaling.

2.4. Phase space (kinematic) and dynamic mass

We now investigate the effects of separately varying the mass entering the $\chi(n)$ variable taking into account the phase space constraints and the mass value entering the hard scattering cross section $\widehat{\sigma}(m)$. We call the former mass parameter "phase space (kinematic) mass" and the latter "dynamic mass".

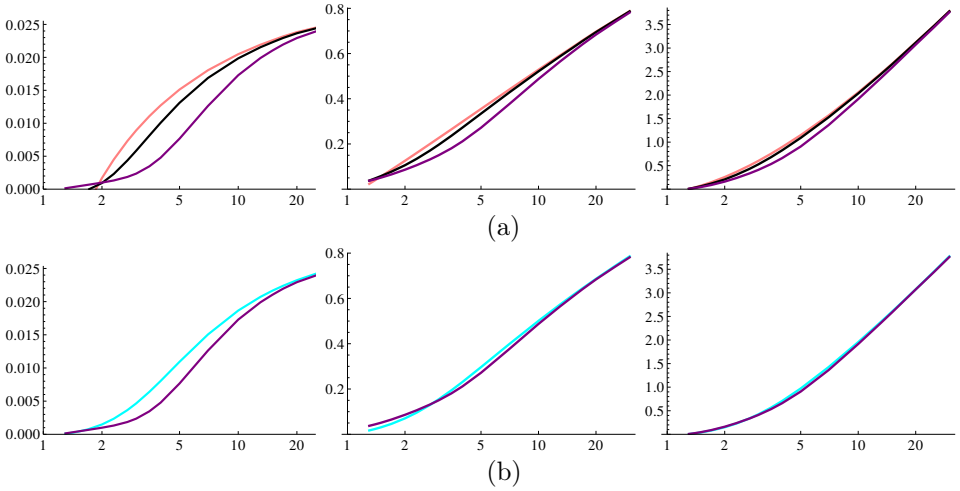

Fig. 3. Comparison of phase space (kinematic) and dynamic mass effects. (a) Comparison of $F_2^c(x, Q)$ *vs.* Q for the NLO ACOT calculation for $x = \{10^{-1}, 10^{-3}, 10^{-5}\}$ (left to right) using zero dynamic mass $[\widehat{\sigma}(m = 0)]$ to show the effect of n scaling; from top to bottom $n = \{0, 1, 2\}$ (pink, black, purple). (b) Comparison of $F_2^c(x, Q)$ *vs.* Q for the NLO ACOT calculation for $x = \{10^{-1}, 10^{-3}, 10^{-5}\}$ (left to right). Here we keep the scaling fixed $n = 2$ and compare the effect of varying the dynamic mass in the Wilson coefficient. The upper (cyan) curve uses a non-zero dynamic mass $[\widehat{\sigma}(m = 1.3)]$ and the lower (purple) curve uses a zero dynamic mass $[\widehat{\sigma}(m = 0)]$.

In Fig. 3 (a), we display $F_2^c(x,Q)$ *vs.* Q. The family of 3 curves shows the NLO ACOT calculation with $\chi(n)$ scaling using a zero dynamic mass for the hard scattering. We compare this with Fig. 3 (b) which shows $F_2^c(x,Q)$ in the NLO ACOT scheme using a fixed $n=2$ scaling, but varying the mass used in the hard-scattering cross section. The upper (cyan) curves use a non-zero dynamic mass $[\widehat{\sigma}(m_c=1.3)]$ and the lower (purple) curves have been obtained with a vanishing dynamic mass $[\widehat{\sigma}(m_c=0)]$. We observe that the effect of the "dynamic mass" in $\widehat{\sigma}(m_c)$ is only of consequence in the limited region $Q \gtrsim m$, and even in this region the effect is minimal. In contrast, the influence of the phase space (kinematic) mass shown in Fig. 3 (a) is larger than the dynamic mass shown in Fig. 3 (b).

In conclusion, we have shown that (up to $\mathcal{O}(\alpha_S)$) the phase space mass dependence is generally the dominant contribution to the DIS structure functions. Assuming that this observation remains true at higher orders, it is possible to obtain a good approximation of the structure functions in the ACOT scheme at NNLO and N^{3}LO using the massless Wilson coefficients together with a non-zero phase space mass entering via the $\chi(n)$-prescription.

2.5. Other massive schemes

There are a number of other schemes for incorporating the heavy quark mass terms, and we briefly note a few examples. The Thorne–Roberts (TR) scheme [14, 15] and its derivatives (TR') are designed to provide a smooth threshold behavior, and this is implemented by including pieces of the higher order contributions. The FONLL scheme [16] was originally developed to match fixed order calculations with resumed ones in the case of heavy quark hadroproduction; this approach has been generalized and applied to other applications including DIS structure functions [17]. Details and comparisons of these approached is outlined in the 2009 Les Houches Workshop report [18].

3. ACOT scheme beyond NLO

In Sec. 2.4, we have shown using the NLO full ACOT scheme that the dominant mass effects are those coming from the phase space which can be taken into account via a generalized slow-rescaling $\chi(n)$-prescription. Assuming that a similar relation remains true at higher orders one can construct the following approximation to the full ACOT result up to N^{3}LO ($\mathcal{O}(\alpha_S^3)$)

$$\text{ACOT}\left[\mathcal{O}\left(\alpha_S^{0+1+2+3}\right)\right] \simeq \text{ACOT}\left[\mathcal{O}\left(\alpha_S^{0+1}\right)\right] + \text{ZM-VFNS}_\chi\left[\mathcal{O}\left(\alpha_S^{2+3}\right)\right]. \tag{4}$$

Here, the massless Wilson coefficients at $\mathcal{O}(\alpha\,\alpha_S^2)$ and $\mathcal{O}(\alpha\,\alpha_S^3)$ are substituted for the Wilson coefficients in the ACOT scheme as the corresponding massive coefficients have not yet been computed.

There has been a calculation of neutral current electroproduction (equal quark masses, vector coupling) of heavy quarks at this order by Smith and van Neerven [19] in the FFNS which could be used to obtain the massive Wilson coefficients in the S-ACOT scheme by applying appropriate collinear subtraction terms[4]; however, this is beyond the scope of this paper. For charge current case massive calculations are available at order $\mathcal{O}(\alpha\,\alpha_S)$ [21, 22, 23] and partial results at order $\mathcal{O}(\alpha\,\alpha_S^2)$ [24].

Here, we argue that the massless Wilson coefficients at $\mathcal{O}(\alpha\,\alpha_S^2)$ together with a $\chi(n)$-prescription provide a very good approximation of the exact result. At worst, the maximum error would be of order $\mathcal{O}(\alpha\,\alpha_S^2 \times [m^2/Q^2])$. However, based on the arguments of Sec. 2.4 we expect the inclusion of the phase space mass effects to contain the dominant higher order contributions so that the actual error should be substantially smaller.

The massless higher order coefficient functions for the DIS structure function F_2 via photon exchange can be found in Refs. [25, 26, 27, 28, 29, 30, 31, 32, 33, 34]. The expressions for the structure function F_L have been calculated in Refs. [35, 29, 31, 36, 33].

We now consider our choice for the appropriate generalized $\chi(n)$-rescaling variable. For the purposes of this study, we will vary the phase space mass using the $\chi(n)$ rescaling with $n = \{0, 1, 2\}$. While $n = 0$ corresponds to the massless case (no rescaling), it is not obvious whether $n = 1$ or $n = 2$ is the preferred rescaling choice for higher orders. Thus, we will use the range between $n = 1$ and $n = 2$ as a measure of our theoretical uncertainty arising from this ambiguity.

4. Results

We now present our results for the F_2 and F_L structure functions calculated at N^{3}LO in the extended ACOT scheme. The initial PDFs, based on the Les Houches benchmark set [37] are evolved using the QCDNUM program [38]. In the calculation we set $m_c = 1.3\,\text{GeV}$, $m_b = 4.5\,\text{GeV}$ and $\alpha_S(M_Z) = 0.118$.

In figures 4 (a) and 4 (b), we display the structure functions F_2 and F_L, respectively, for selected x values as a function of Q. Each plot has three curves which are computed using n-scalings of $\{0, 1, 2\}$. We observe that the effect of the n-scaling is negligible except for very small Q values. This result is in part because the heavy quarks are only a fraction of the total structure function, and the effects of the n-scaling are reduced at larger Q values.

[4] For the original ACOT scheme it would then still be necessary to compute the massive Wilson coefficients for the heavy quark initiated subprocess at $\mathcal{O}(\alpha\,\alpha_S^2)$. See Refs. [12, 20] for details.

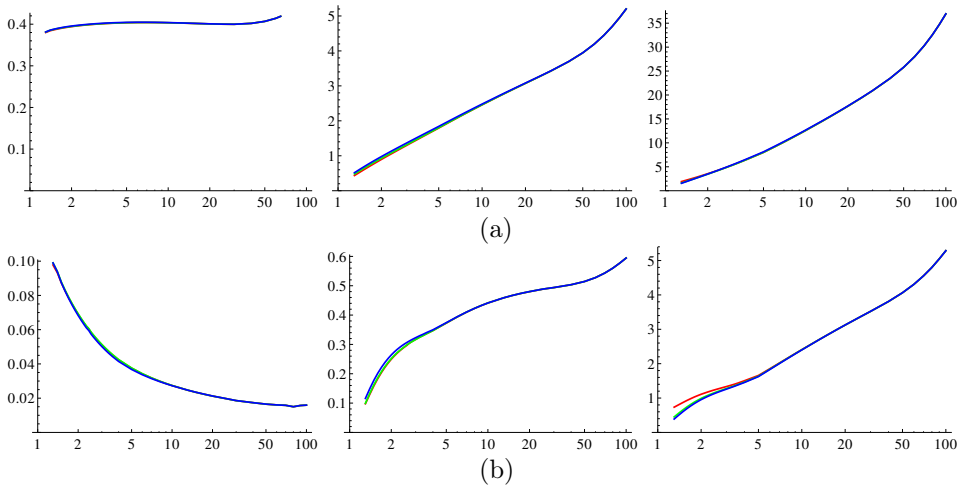

Fig. 4. $F_{2,\mathrm{L}}$ *vs.* Q at N^{3}LO for fixed $x = \{10^{-1}, 10^{-3}, 10^{-5}\}$ (left to right). The three lines show the scaling variable: $n = \{0, 1, 2\}$ (red, green, blue). We observe the effect of the n-scaling is negligible except for very small Q values. (a) F_2 *vs.* Q. (b) F_{L} *vs.* Q.

In Ref. [3] we magnify the small Q region of F_{L} of Fig. 4 (b) for $x = 10^{-5}$, where the effects of using different scalings are largest. We can see that for inclusive observables, the $n = 1$ and $n = 2$ scalings give nearly identical results, but they differ from the massless case ($n = 0$). This result, together with the observation that at NLO kinematic mass effects are dominant, suggests that the error we have in our approach is relatively small and approximated by the band between $n = 1$ and $n = 2$ results.

We can investigate the effects of the $\chi(n)$-scaling in more details by examining the flavor decomposition of the structure functions. In figures 5 (a) and 5 (b), we display the fractional contributions of quark flavors to the structure functions $F_{2,\mathrm{L}}$ for selected n-scaling values as a function of Q. We observe the n-scaling reduces the relative contributions of charm and bottom at low Q scales. For example, without any n-scaling ($n = 0$) we find the charm and bottom quarks contribute an unusually large fraction at very low scales ($Q \sim m_c$) as they are (incorrectly) treated as massless partons in this region. The result of the different n-scalings ($n = 1, 2$) is to introduce a kinematic penalty which properly suppresses the contribution of these heavy quarks in the low Q region. In the following, we will generally use the $n = 2$ scaling for our comparisons.

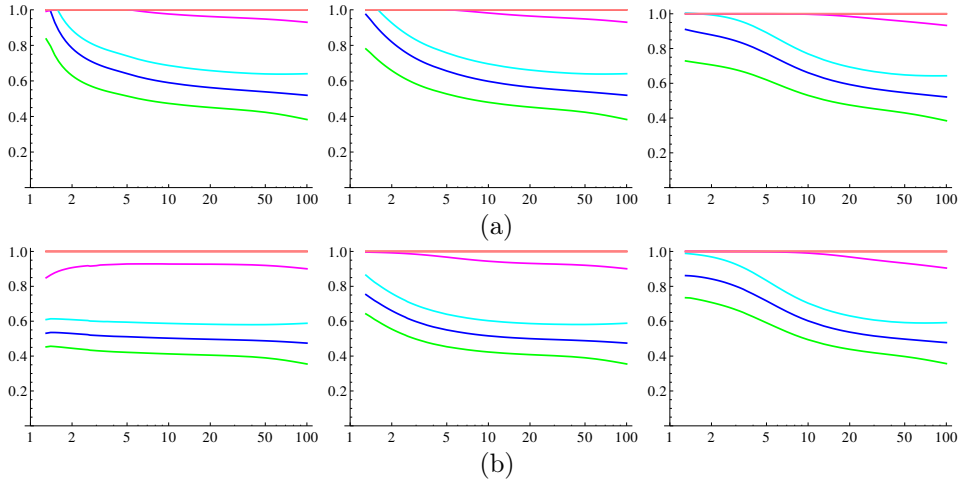

Fig. 5. Effect of $\chi(n)$-scaling for $n = \{0, 1, 2\}$ (left to right) at N^{3}LO for fixed $x = \{10^{-3}\}$. Reading from the bottom, we have fractional contribution for each (final-state) quark flavor to $F^j_{2,\mathrm{L}}/F_{2,\mathrm{L}}$ *vs.* Q from $\{u, d, s, c, b\}$ (green, blue, cyan, magenta, pink). (a) F^j_2/F_2 *vs.* Q. (b) $F^j_{\mathrm{L}}/F_{\mathrm{L}}$ *vs.* Q.

In figures 6 (a) and 6 (b), we display the fractional contributions for the initial-state quarks (i) to the structure functions F_2 and F_{L}, respectively, for selected x values as a function of Q; here we have used $n = 2$ scaling. Reading from the bottom, we have the cumulative contributions from the $\{g, u, d, s, c, b\}$. We observe that for large x and low Q the heavy flavor contributions are minimal. For example, for $x = 10^{-1}$ we see the contribution of the u quark comprises $\sim 80\%$ of the F_2 structure function at low Q. In contrast, at $x = 10^{-5}$ and large Q, we see the F_2 contributions of the u quark and c quark are comparable (as they both couple with a factor $4/9$), and the d quark and s quark are comparable (as they both couple with a factor $1/9$). It is notable that the gluon contribution to F_{L} is significant. For $x = 10^{-1}$ this is roughly 40% throughout the Q range, and can be even larger for smaller x values.

In figures 7 (a) and 7 (b), we display the fractional contributions for the final-state quarks (j) to the structure functions F_2 and F_{L}, respectively, for selected x values as a function of Q; here we have used $n = 2$ scaling. Reading from the bottom, we have the cumulative contributions from the $\{u, d, s, c, b\}$. Again, we observe that for large x and low Q the heavy flavor contributions are minimal, but these can grow quickly as we move to smaller x and larger Q.

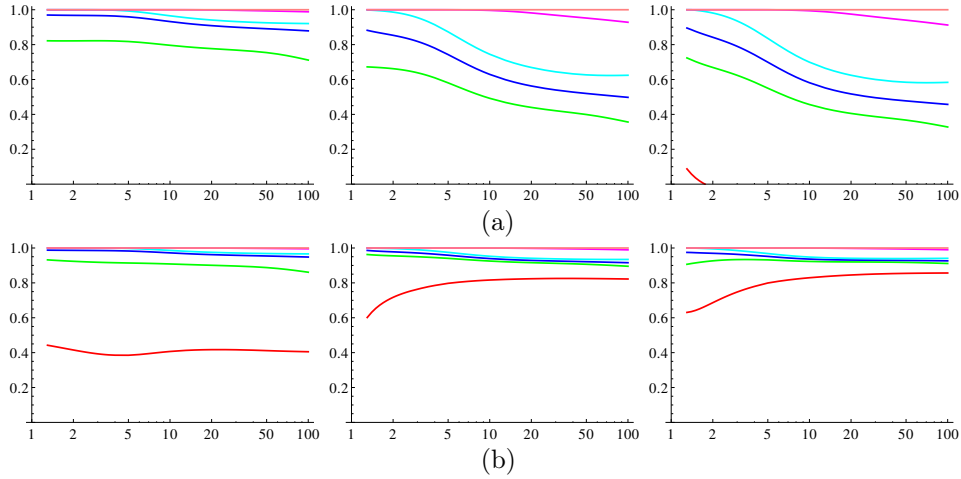

Fig. 6. Fractional flavor decomposition of "initial-state" $F^i_{2,\mathrm{L}}/F_{2,\mathrm{L}}$ *vs.* Q at N^{3}LO for $x = \{10^{-1}, 10^{-3}, 10^{-5}\}$ (left to right) for $n = 2$ scaling. Reading from the bottom, we plot the cumulative contributions to $F_{2,\mathrm{L}}$ from $\{g, u, d, s, c, b\}$, (red, green, blue, cyan, magenta, pink). (a) F^i_2/F_2 *vs.* Q. (b) $F^i_{\mathrm{L}}/F_{\mathrm{L}}$ *vs.* Q.

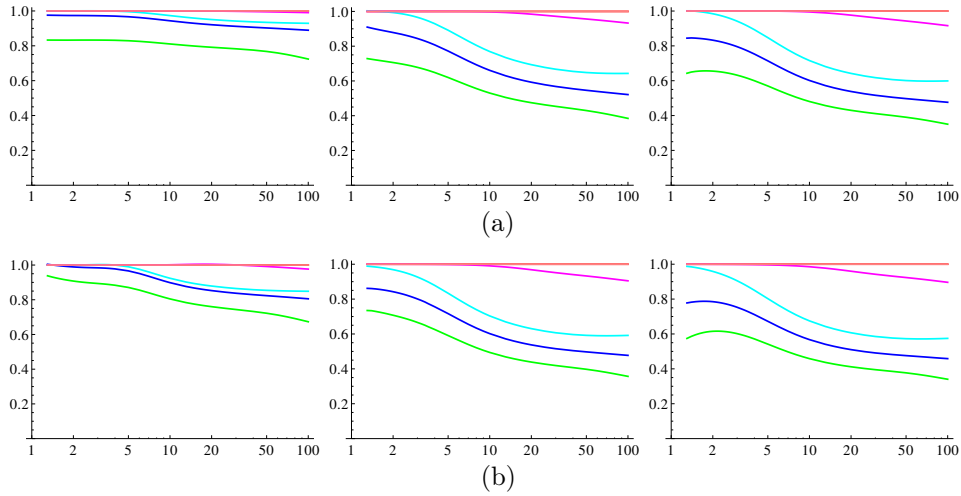

Fig. 7. Fractional contribution for each quark flavor to $F^j_{2,\mathrm{L}}/F_{2,\mathrm{L}}$ *vs.* Q at N^{3}LO for fixed $x = \{10^{-1}, 10^{-3}, 10^{-5}\}$ (left to right). Results are displayed for $n = 2$ scaling. Reading from the bottom, we have the cumulative contributions from the $\{u, d, s, c, b\}$ (green, blue, cyan, magenta, pink). (a) F^j_2/F_2 *vs.* Q. (b) $F^j_{\mathrm{L}}/F_{\mathrm{L}}$ *vs.* Q.

In figure 8 (a), we display the results for F_2 *vs.* Q computed at various orders. For large x (*cf.* $x = 0.1$) we find the perturbative calculation is particularly stable; we see that the LO result is within 20% of the others at small Q, and within 5% at large Q. The NLO is within 2% at small Q, and indistinguishable from the NNLO and N^{3}LO for Q values above $\sim 10\,\text{GeV}$. The NNLO and N^{3}LO results are essentially identical throughout the kinematic range. For smaller x values (10^{-3}, 10^{-5}), the contribution of the higher order terms increases. Here, the NNLO and N^{3}LO coincide for Q values above $\sim 5\,\text{GeV}$, but the NLO result can differ by $\sim 5\%$.

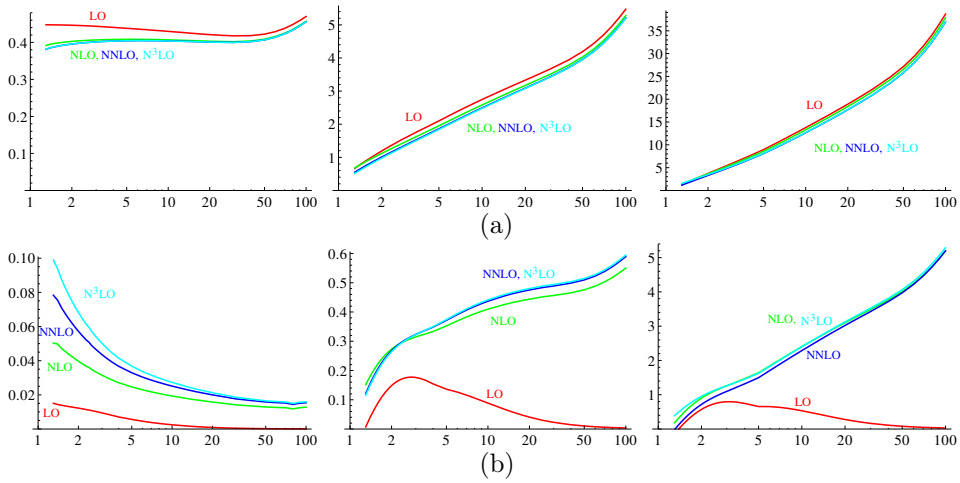

Fig. 8. $F_{2,\text{L}}$ *vs.* Q at {LO, NLO, NNLO, N^{3}LO} (red, green, blue, cyan) for fixed $x = \{10^{-1}, 10^{-3}, 10^{-5}\}$ (left to right) for $n = 2$ scaling. (a) F_2 *vs.* Q. (b) F_L *vs.* Q.

In Figure 8 (b), we display the results for F_L *vs.* Q computed at various orders. In contrast to F_2, we find the NLO corrections are large for F_L; this is because the LO F_L contribution (which violates the Callan–Gross relation) is suppressed by (m^2/Q^2) compared to the dominant gluon contributions which enter at NLO. Consequently, we observe (as expected) that the LO result for F_L receives large contributions from the higher order terms. Essentially, the NLO is the first non-trivial order for F_L, and the subsequent contributions then converge. For example, at large x (*cf.* $x = 0.1$) for $Q \sim 10\,\text{GeV}$ we find the NLO result yields ~ 60 to 80% of the total, the NNLO is a $\sim 20\%$ correction, and the N^{3}LO is a $\sim 10\%$ correction. For lower x values (10^{-3}, 10^{-5}), the convergence of the perturbative series improves, and the NLO results is within $\sim 10\%$ of the N^{3}LO result. Curiously, for $x = 10^{-5}$ the NNLO and N^{3}LO roughly compensate each other so that the NLO and the N^{3}LO match quite closely for $Q \geq 2\,\text{GeV}$.

While the calculation of $F_{\rm L}$ is certainly more challenging, examining Fig. 1 we see that for most of the relevant kinematic range probed by HERA the theoretical calculation is quite stable. For example, in the high Q^2 region where HERA is probing intermediate x values ($x \sim 10^{-3}$) the spread of the $\chi(n)$ scalings is small. The challenge arises in the low Q region ($Q \sim 2\,\text{GeV}$), where the x values are $\sim 10^{-4}$; in this region, there is some spread between the various curves at the lowest x value ($\sim 10^{-5}$), but for $x \sim 10^{-3}$ this is greatly reduced.

5. Conclusions

We extended the ACOT calculation for DIS structure functions to N^{3}LO by combining the exact ACOT scheme at NLO with a $\chi(n)$-rescaling which allows us to include the leading mass dependence at NNLO and N^{3}LO. Using the full ACOT calculation at NLO, we demonstrated that the heavy quarks mass dependence for the DIS structure functions is dominated by the kinematic mass contributions, and this can be implemented via a generalized $\chi(n)$-rescaling prescription.

We studied the F_2 and $F_{\rm L}$ structure functions as a function of x and Q. We examined the flavor decomposition of these structure functions, and verified that the heavy quarks were appropriately suppressed in the low Q region. We found the results for F_2 were very stable across the full kinematic range for $\{x, Q\}$, and the contributions from the NNLO and N^{3}LO terms were small. For $F_{\rm L}$, the higher order terms gave a proportionally larger contribution (due to the suppression of the LO term from the Callan–Gross relation); nevertheless, the contributions from the NNLO and N^{3}LO terms were generally small in the region probed by HERA.

The result of this calculation was to obtain precise predictions for the inclusive F_2 and $F_{\rm L}$ structure functions which can be used to analyze the HERA data.

We thank M. Botje, A.M. Cooper-Sarkar, A. Glazov, C. Keppel, J.G. Morfín, P. Nadolsky, M. Guzzi, J.F. Owens, V.A. Radescu, and A. Vogt for discussions. F.I.O., I.S., and J.Y.Y. acknowledge the hospitality of CERN, DESY, Fermilab, and Les Houches, where a portion of this work was performed. This work was partially supported by the U.S. Department of Energy under grant DE-FG02-04ER41299, and the Lightner-Sams Foundation. F.I.O. thanks the Galileo Galilei Institute for Theoretical Physics for their hospitality and the INFN for partial support during the completion of this work. The research of T.S. is supported by a fellowship from the Théorie LHC France initiative funded by the CNRS/IN2P3. This work has been supported by *Projet international de cooperation scientifique* PICS05854 between France and the USA. The work of J.Y.Y. was supported by the Deutsche Forschungsgemeinschaft (DFG) through grant No. YU 118/1-1.

REFERENCES

[1] I. Schienbein *et al.*, *J. Phys. G* **35**, 053101 (2008) [arXiv:0709.1775v2 [hep-ph]].

[2] H1 and ZEUS collaborations, Combined Measurement of the Inclusive e^+p Scattering Cross Sections at HERA for Reduced Proton Beam Energy Runs and Determination of Structure Function F_L, 2010, H1prelim-10-044, ZEUS-prel-10-008.

[3] T. Stavreva *et al.*, *Phys. Rev.* **D85**, 114014 (2012) [arXiv:1203.0282v3 [hep-ph]].

[4] M.A.G. Aivazis, F.I. Olness, W.K. Tung, *Phys. Rev.* **D50**, 3085 (1994) [arXiv:hep-ph/9312318v2].

[5] M.A.G. Aivazis, J.C. Collins, F.I. Olness, W.K. Tung, *Phys. Rev.* **D50**, 3102 (1994) [arXiv:hep-ph/9312319v2].

[6] J.C. Collins, *Phys. Rev.* **D58**, 094002 (1998) [arXiv:hep-ph/9806259v1].

[7] S. Kretzer, I. Schienbein, *Phys. Rev.* **D58**, 094035 (1998) [arXiv:hep-ph/9805233v2].

[8] M. Krämer, F.I. Olness, D.E. Soper, *Phys. Rev.* **D62**, 096007 (2000) [arXiv:hep-ph/0003035v1].

[9] R.M. Barnett, *Phys. Rev. Lett.* **36**, 1163 (1976).

[10] J. Amundson *et al.*, in: Proceedings of 6th International Workshop on Deep Inelastic Scattering and QCD (DIS 98), Brussels, Belgium, 4–8 Apr, 1998.

[11] W.K. Tung, S. Kretzer, C. Schmidt, *J. Phys. G* **28**, 983 (2002) [arXiv:hep-ph/0110247v1].

[12] M. Guzzi, P.M. Nadolsky, H.-L. Lai, C.-P. Yuan, arXiv:1108.5112v2 [hep-ph].

[13] P.M. Nadolsky, W.-K. Tung, *Phys. Rev.* **D79**, 113014 (2009) [arXiv:0903.2667v4 [hep-ph]].

[14] R. Thorne, R. Roberts, *Phys. Rev.* **D57**, 6871 (1998) [arXiv:hep-ph/9709442v1].

[15] R. Thorne, R. Roberts, *Phys. Lett.* **B421**, 303 (1998) [arXiv:hep-ph/9711223v1].

[16] M. Cacciari, M. Greco, P. Nason, *J. High Energy Phys.* **9805**, 007 (1998) [arXiv:hep-ph/9803400v1].

[17] S. Forte, E. Laenen, P. Nason, J. Rojo, *Nucl. Phys.* **B834**, 116 (2010) [arXiv:1001.2312v2 [hep-ph]].

[18] [SM and NLO Multileg Working Group Collaboration], J. Andersen *et al.*, arXiv:1003.1241v1 [hep-ph].

[19] E. Laenen, S. Riemersma, J. Smith, W.L. van Neerven, *Nucl. Phys.* **B392**, 162 (1993).

[20] M. Guzzi, P.M. Nadolsky, H.-L. Lai, C.P. Yuan, arXiv:1108.4008v1 [hep-ph].

[21] T. Gottschalk, *Phys. Rev.* **D23**, 56 (1981).

[22] M. Gluck, S. Kretzer, E. Reya, *Phys. Lett.* **B380**, 171 (1996) [arXiv:hep-ph/9603304v1].

[23] J. Blumlein, A. Hasselhuhn, P. Kovacikova, S. Moch, *Phys. Lett.* **B700**, 294 (2011) [arXiv:1104.3449v1 [hep-ph]].

[24] M. Buza, W.L. van Neerven, *Nucl. Phys.* **B500**, 301 (1997) [arXiv:hep-ph/9702242v1].

[25] W. Furmanski, R. Petronzio, *Z. Phys.* **C11**, 293 (1982).

[26] W.A. Bardeen, A.J. Buras, D.W. Duke, T. Muta, *Phys. Rev.* **D18**, 3998 (1978).

[27] G. Altarelli, R.K. Ellis, G. Martinelli, *Nucl. Phys.* **B143**, 521 (1978).

[28] W.L. van Neerven, E.B. Zijlstra, *Phys. Lett.* **B272**, 127 (1991).

[29] E.B. Zijlstra, W.L. van Neerven, *Phys. Lett.* **B273**, 476 (1991).

[30] E.B. Zijlstra, W.L. van Neerven, *Nucl. Phys.* **B383**, 525 (1992).

[31] W.L. van Neerven, A. Vogt, *Nucl. Phys.* **B568**, 263 (2000) [arXiv:hep-ph/9907472v1].

[32] W.L. van Neerven, A. Vogt, *Nucl. Phys.* **B588**, 345 (2000) [arXiv:hep-ph/0006154v1].

[33] J.A.M. Vermaseren, A. Vogt, S. Moch, *Nucl. Phys.* **B724**, 3 (2005) [arXiv:hep-ph/0504242v1].

[34] S. Moch, J.A.M. Vermaseren, A. Vogt, *Nucl. Phys.* **B646**, 181 (2002) [arXiv:hep-ph/0209100v1].

[35] J. Sanchez Guillen *et al.*, *Nucl. Phys.* **B353**, 337 (1991).

[36] S. Moch, J.A.M. Vermaseren, A. Vogt, *Phys. Lett.* **B606**, 123 (2005) [arXiv:hep-ph/0411112v2].

[37] W. Giele *et al.*, arXiv:hep-ph/0204316v1.

[38] M. Botje, *Comput. Phys. Commun.* **182**, 490 (2011) [arXiv:1005.1481v3 [hep-ph]].